PHYSICAL REVIEW B **101**, 165116 (2020)

Magnetic transition due to the inter-singlet spin-exchange interaction and elastic softening by the interplay of electric quadrupoles in the distorted kagome lattice antiferromagnet $Tb_3Ru_4Al_{12}$

Isao Ishii,* Takuyou Mizuno, Soichiro Kumano, Tomohiro Umeno, Daichi Suzuki, Yuki Kurata, and Takashi Suzuki†
Department of Quantum Matter, AdSM, Hiroshima University, Higashi-Hiroshima 739-8530, Japan

Denis I. Gorbunov
Hochfeld-Magnetlabor Dresden (HLD-EMFL) and Würzburg-Dresden Cluster of Excellence ct.qmat, Helmholtz-Zentrum Dresden-Rossendorf, D-01328 Dresden, Germany

Margarida S. Henriques and Alexander V. Andreev
FZU Institute of Physics, Czech Academy of Sciences, Na Slovance 2, 182 21 Prague, Czech Republic

(Received 10 January 2020; revised manuscript received 26 February 2020; accepted 26 March 2020; published 15 April 2020)

The distorted kagome lattice antiferromagnet $Tb_3Ru_4Al_{12}$ with a hexagonal structure has the Néel temperature $T_N = 22$ K. To clarify the $4f$-electronic state and an influence of electric quadrupoles in $Tb_3Ru_4Al_{12}$, ultrasonic measurements on a single-crystalline sample at zero magnetic field and under fields were carried. A characteristic elastic softening of the transverse modulus C_{66} originating from a quadrupole interaction was found. The crystal electric field parameters were determined to reproduce C_{66}, magnetic susceptibilities, and magnetization curves. The obtained level scheme is that the ground and first excited states are singlets, despite the existence of both the magnetic transition and the quadrupole interaction, indicating that $Tb_3Ru_4Al_{12}$ is a curious compound. The positive sign of the quadrupole-quadrupole coupling constant for C_{66} indicates a ferroquadrupolar-type interaction of the electric quadrupole O_{xy} or O_2^2. The anisotropic magnetic field dependencies of T_N in the field along [100] and [001] were also clarified.

DOI: 10.1103/PhysRevB.101.165116

I. INTRODUCTION

Exotic physical properties arising from the spin and orbital degrees of freedom, such as magnetic ordering accompanied by complex magnetic structures and multipolar ordering, have attracted much attention in rare-earth compounds with localized f electrons [1–4]. The electric quadrupole, which is caused by the orbital degrees of freedom, often plays an important role for physical properties under a crystal electric field (CEF). The ternary rare-earth compounds $R_3Ru_4Al_{12}$ (R: rare-earth, Y, and U) with the hexagonal $Gd_3Ru_4Al_{12}$-type structure (space group $P6_3/mmc$) at room temperature have a distorted kagome net consisting of the R atoms in (001) planes [5,6]. The R-Al and Ru-Al layers are stacked along [001] alternately. This series has been primarily studied in terms of magnetism, for instance, an antiferromagnetic and a field-induced quadrupolar orderings in $Dy_3Ru_4Al_{12}$ and a helical ordering of spin trimers in $Gd_3Ru_4Al_{12}$ [7–24].

The Tb-based $Tb_3Ru_4Al_{12}$ undergoes an antiferromagnetic ordering at $T_N = 22$ K reported by the specific heat and following measurements [12,13]. The electrical resistivity shows a metallic behavior. The temperature T dependence of the magnetization increases steeply below T_N under a magnetic field H at 0.1 T along [001] in contrast to those in the (001) plane which decrease below T_N at 5 T. The magnetization M curves display two- and one-step anomalies accompanied by hysteresis in H around 1 T along [001] and around 6–7 T in the (001) plane, respectively [12,14]. For the phase transition at T_N, an incommensurate-type long-range antiferromagnetic (AFM) ordering was proposed by neutron diffraction experiments [15]. The ordered magnetic structure is that reduced Tb magnetic moments are almost aligned along [001] forming a ferromagnetic-type state in the unit cell and are slightly canted toward [120]. A stripelike magnetic domain structure consisting of one spin-up and two spin-down states, therefore AFM ordering, was reported. In addition, spin-glass-like features were also suggested below about 17 K [14,15].

The magnetic susceptibility χ obeys the Curie-Weiss law above 100 and 170 K along [100] and [001], respectively [12]. The effective magnetic moments were determined to be 10.4 and 10.7 μ_B, respectively, which are around the value for the free Tb^{3+} ion (9.72 μ_B). Here, a contribution from the Ru $4d$ electrons was suggested as a reason to have effective magnetic moments larger than the theoretical value. These results suggest that $4f$ electrons of the Tb^{3+} ion are almost localized and there is the CEF effect in $Tb_3Ru_4Al_{12}$. The 13-fold multiplet of the Tb^{3+} ion (the total angular momentum

*ish@hiroshima-u.ac.jp
†Also at Cryogenics and Instrumental Analysis Division, N-BARD, Hiroshima University, Higashi-Hiroshima 739-8530, Japan; tsuzuki@hiroshima-u.ac.jp

2469-9950/2020/101(16)/165116(7)

$J = 6$) splits into five singlets ($2\Gamma_1$, Γ_2, Γ_3, and Γ_4) and four doublets ($2\Gamma_5$ and $2\Gamma_6$) under the hexagonal CEF determined by the group theory using the character table for D_{6h} point group, where Γ_l is the irreducible representation.

In our recent works, it was clarified that a quadrupole interaction by electric quadrupoles under the hexagonal CEF plays an important role for understanding physical properties in the $R_3Ru_4Al_{12}$ system [19,20,22,24]. The ultrasonic technique is a powerful tool for investigating the quadrupole interaction because a strain induced by ultrasound bilinearly couples to a corresponding quadrupole moment [25–35]. Here, the transverse modulus C_{66} (C_{44}) is the linear responses to the ε_{xy} and $\varepsilon_{xx} - \varepsilon_{yy}$ (ε_{yz} and ε_{zx}) strains which couple to the quadrupoles O_{xy} and O_2^2 (O_{yz} and O_{zx}), respectively, in the hexagonal symmetry. The CEF analyses based on the elastic properties in addition to the magnetic properties make the results more precise [20,22,24,33,34,36]. In this work, to clarify the $4f$-electronic state under the CEF and an influence of the quadrupole interaction in $Tb_3Ru_4Al_{12}$, we measured the elastic moduli using ultrasonic technique at zero magnetic field and under fields, and determined the CEF level scheme and the H-T phase diagrams.

II. EXPERIMENTAL DETAILS

Single crystal of $Tb_3Ru_4Al_{12}$ was grown by a modified Czochralski method in triarc furnace and the lattice parameters were determined to be $a = 8.784$ Å and $c = 9.542$ Å at room temperature [12]. The orientation of the single crystal was confirmed by back-scattered Laue diffraction patterns. The elastic moduli C_{11}, C_{33}, C_{44}, and C_{66} were measured as a function of T from 2 to 150 K and of H up to 10 T using a phase-comparison-type pulse-echo method and a superconducting magnet [37]. The moduli C_{11} and C_{33} are the longitudinal modes with the propagation and polarization directions along [100] and [001], respectively. The transverse moduli C_{44} and C_{66} are the modes propagating along [100] with the polarization direction along [001] and in the (001) plane, respectively. The absolute value of the elastic modulus C was calculated using the equation $C = \rho v^2$ with a room temperature mass density $\rho = 6.276$ g/cm^3, where v is the sound velocity in the sample. We used $LiNbO_3$ transducers with the fundamental resonance frequency of about 30 MHz. Magnetic measurements were performed by using a commercial Magnetic Property Measurement System [(MPMS) Quantum Design] down to 2 K and up to 5 T.

III. RESULTS AND DISCUSSION

A. Magnetic susceptibility

Figures 1(a) and 1(b) show the T dependencies of χ along [100] and [001], respectively, in $Tb_3Ru_4Al_{12}$. χ along [100] at 0.1 T increases with decreasing T and changes the slope upward at T_N. Above 0.5 T χ tends to be reduced below T_N. T_N decreases with increasing H and survives up to 5 T along $H||[100]$. On the other hand, an abrupt enhancement below T_N is observed in χ along [001] at 0.1 T, as shown in Fig. 1(b). With increasing H, T_N decreases rapidly and becomes unclear above 1.5 T. The magnetic behaviors of the data at 5 T along

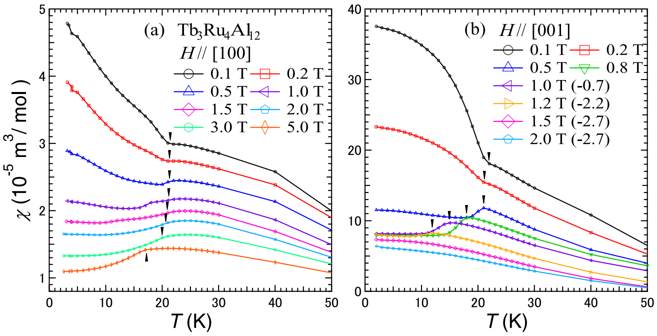

FIG. 1. T dependencies of the magnetic susceptibility χ along (a) [100] and (b) [001] on field cooling at elevated magnetic fields. The curves along [001] above 1 T are vertically offset for easier viewing of each data curve. The arrow indicates the phase transition at T_N.

$H||[100]$ and at 0.1 T along $H||[001]$ are consistent with the data previously reported [12].

B. Elastic modulus

The T dependencies of the longitudinal elastic moduli C_{11} and C_{33} in $Tb_3Ru_4Al_{12}$ are shown in Fig. 2. Both moduli harden monotonically with decreasing T at high temperatures. The modulus C_{11} displays a slight softening below 50 K. At T_N an elastic hardening is observed in both moduli.

Figure 3 shows the T dependencies of the transverse elastic moduli C_{44} and C_{66} in $Tb_3Ru_4Al_{12}$. Both moduli increase monotonically on cooling down to 50 K. With further decreasing T, C_{44} exhibits a change of the slope at T_N. By contrast, an obvious elastic softening is detected below 50 K in C_{66}. The softening stops at T_N and C_{66} starts to harden below T_N. No obvious anomaly is observed around 17 K owing to spin-glass-like features reported [14,15].

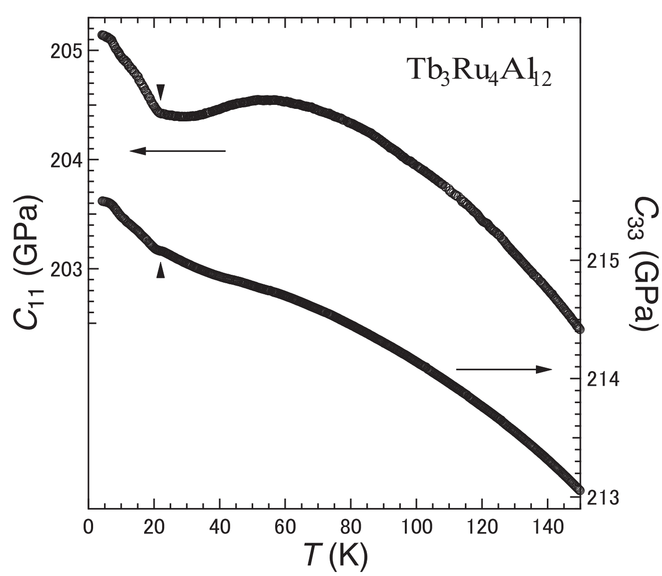

FIG. 2. T dependencies of the longitudinal elastic moduli C_{11} and C_{33} in $Tb_3Ru_4Al_{12}$. The vertical arrow indicates the phase transition at T_N.

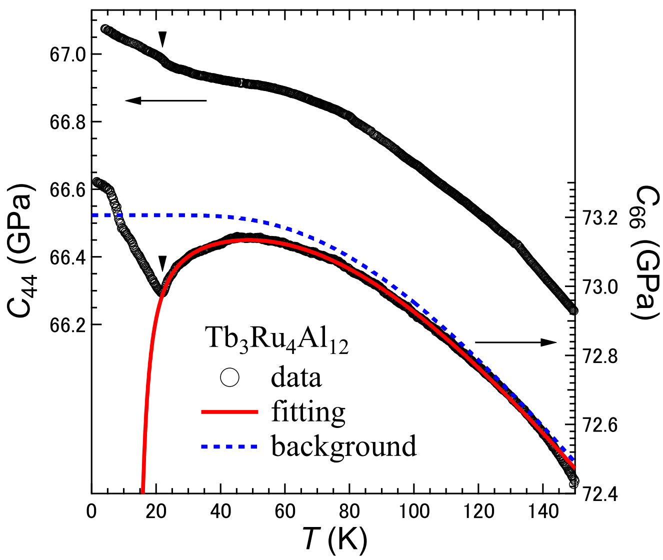

FIG. 3. T dependencies of the transverse elastic moduli C_{44} and C_{66} in $Tb_3Ru_4Al_{12}$. The vertical arrow indicates the phase transition at T_N. The red solid and blue broken curves represent the fitting result and the background stiffness, respectively.

C. Crystal electric field effect

The elastic softening of C_{66} starts from quite higher temperature than T_N, suggesting that the softening is not caused by a precursor or fluctuation of the phase transition. The softening is a characteristic behavior originating from a quadrupole interaction under the CEF. We performed the CEF analyses for the elastic modulus C_{66}, inverse magnetic susceptibilities, and magnetization curves. We considered the effective Hamiltonian $H_{\rm eff}$:

$$\begin{aligned} H_{\rm eff} &= H_{\rm CEF} + H_{\rm Q} + H_{\rm ex} + H_{\rm Zeeman}, \\ H_{\rm CEF} &= B_2^0 O_2^0 + B_4^0 O_4^0 + B_6^0 O_6^0 + B_6^6 O_6^6, \\ H_{\rm Q} &= -\sum_i g_i O_i \varepsilon_i - \sum_i g_i' \langle O_i \rangle O_i \ \ (i = 6), \\ H_{\rm ex} &= -\sum_{j=A,B} J_{\rm ex}^{AB} (\langle J_x \rangle^{(j)} J_x + \langle J_y \rangle^{(j)} J_y + \langle J_z \rangle^{(j)} J_z), \\ H_{\rm Zeeman} &= -g_J \mu_B J H, \end{aligned}$$

where g_i, g_i', O_i, B_m^n, and O_m^n are the strain-quadrupole coupling constant, the quadrupole-quadrupole coupling constant, the quadrupole operator, the CEF parameter, and the Stevens equivalent operator, respectively. $\langle O_i \rangle$, $\langle J_x \rangle$, $\langle J_y \rangle$, and $\langle J_z \rangle$ represent the thermal average of operators. The subscript $i = 6$ denotes xy, and subscripts x, y, and z correspond to [100], [120], and [001], respectively, in the hexagonal symmetry. The quadrupole interaction term $H_{\rm Q}$ is for only C_{66}. The T dependence of the elastic modulus, $C_{ii}(T)$, is represented by the following equation:

$$C_{ii}(T) = C_0 \left[\frac{1 - (N_0 g_i^2 / C_0 + g_i') \chi_s(T)}{1 - g_i' \chi_s(T)} \right],$$

TABLE I. CEF parameters of $Tb_3Ru_4Al_{12}$ in Kelvin.

B_2^0	B_4^0	B_6^0	B_6^6
-1.10	-5.00×10^{-4}	5.00×10^{-6}	-2.65×10^{-3}

where N_0 ($= 9.41 \times 10^{27}$ m^{-3}) is the number density of Tb ions per unit volume at room temperature and χ_s is the so-called strain susceptibility [38]. We adopted the so-called Varshni equation as the T dependence of the background stiffness C_0 [39]:

$$C_0(T) = C_{0\rm K} - \frac{s}{\exp(\theta_{\rm D}/T) - 1},$$

where $C_{0\rm K}$ is the elastic modulus at 0 K, $\theta_{\rm D}$ is the Debye temperature, and s is the fitting parameter [40].

For the calculation of $1/\chi$ and M, we adopted the mean-field term of spin exchange interaction $H_{\rm ex}$ in the AFM ordered state, including a parameter of an intersublattice spin-exchange interaction $J_{\rm ex}^{AB}$, where symbols A and B mean two sublattices [41]. We disregarded an intrasublattice spin-exchange interaction to simplify the analysis. $H_{\rm Zeeman}$ is the Zeeman term. $1/\chi$ and M were calculated using the CEF model in the usual manner [42,43].

The red solid curve in Fig. 3 is the best fit. The softening of C_{66} above T_N is well reproduced by the theoretical curve of the strain susceptibility with fitting parameters listed in Tables I and II. This fitting result reveals that the softening of C_{66} originates from the quadrupole interaction, which is of ferroquadrupolar type because of the positive sign of g'. Figures 4(a) and 4(b) show fitting results of the $1/\chi$ vs T and M vs H data, respectively. The gradient of both $1/\chi$ data and the magnitude of magnetic anisotropy are qualitatively reproduced, as shown in Fig. 4(a). Here, $J_{\rm ex}^{AB} = 1.02$ K was determined to reproduce T_N, and the ferromagnetic interaction of $J_{\rm ex}^{AB}$ is consistent with the results by neutron diffraction studies of which the ferromagnetic interaction exists in the unit cell [15]. If there is no spin-exchange interaction, the absolute values of the calculated results further deviate from the experimental data. A magnetic contribution from the Ru 4d subsystem was supposed in $Tb_3Ru_4Al_{12}$ as well as $Dy_3Ru_4Al_{12}$ [12,16]. The reason why the absolute values of $1/\chi$ are not explicable by the calculation may be owing to an influence of the Ru magnetic moments. On the other hand, M curves shown in Fig. 4(b) are explained by the calculated results except for the two-step anomaly in M along H||[001] [12]. To reproduce the two-step anomaly, a complicated model considering the reported ordered state may be needed.

From these fittings, we determined the CEF level scheme: the ground singlet Γ_1, the first excited singlet Γ_2 at 13 K, the

TABLE II. Fitting parameters of C_{66}: $|g_i|$ (K), g_i' (K), $C_{0\rm K}$ (GPa), $\theta_{\rm D}$ (K), and s (GPa). We used the value of $\theta_{\rm D}$ obtained from the electrical resistivity [12].

	$\|g_i\|$	g_i'	$C_{0\rm K}$	$\theta_{\rm D}$	s
C_{66}	15.2	0.41	73.2	281	3.94

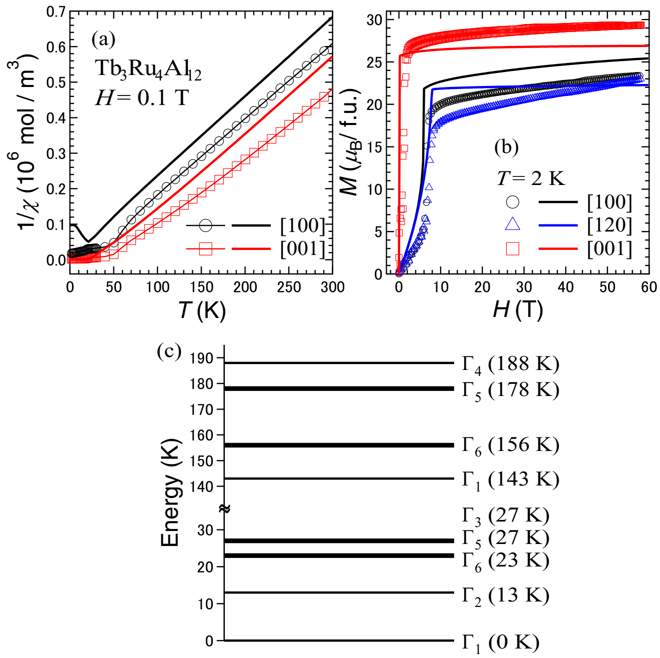

FIG. 4. (a) T dependencies of the inverse magnetic susceptibility at 0.1 T. (b) Magnetization curves at 2 K. The calculated results are represented by solid curves. The data of M are the same with the data previously reported [12]. (c) The $4f$-level scheme of $Tb_3Ru_4Al_{12}$ obtained from the CEF parameters listed in Table I.

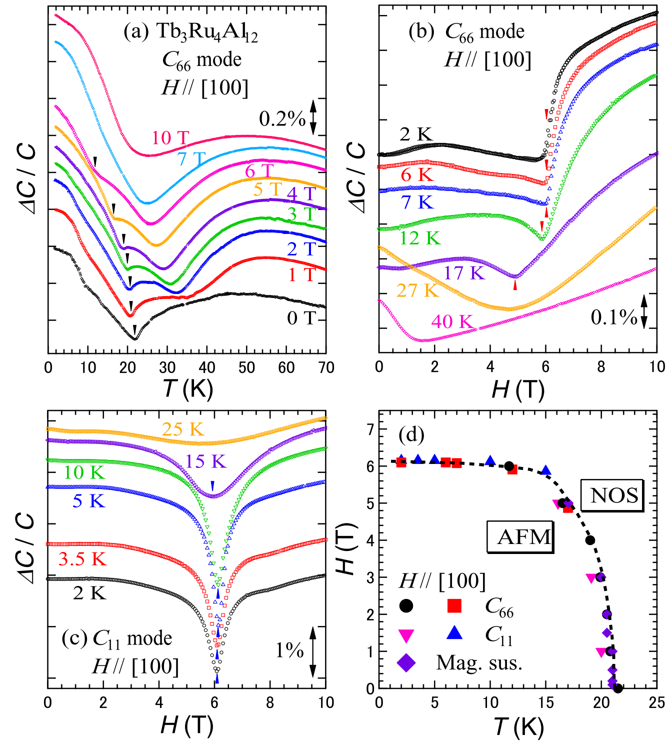

FIG. 5. T and H dependencies of the elastic moduli (a) and (b) C_{66} and (c) C_{11} along $H||[100]$ at various conditions in $Tb_3Ru_4Al_{12}$. The data are plotted adding a constant value to easily see each data curve. The arrow indicates the phase transition at T_N. (d) The H-T phase diagram along $H||[100]$. The broken curve is a guide for the eyes. Black circles and magenta down triangles (red squares and blue up triangles) represent the phase boundary determined by the T (H) dependencies of the elastic moduli. NOS indicates the nonordered state.

second excited doublet Γ_6 at 23 K, and so on, as shown in Fig. 4(c). Below 22 K which corresponds to the temperature of the AFM ordering, two singlets Γ_1 and Γ_2, possessing only interlevel spin interaction of J_z, exist at zero magnetic field. This result is consistent with the ordered state in $Tb_3Ru_4Al_{12}$.

The ground singlet Γ_1 has no quadrupole degeneracy. The softening of C_{66} above T_N is caused by an interlevel quadrupole interaction between the ground singlet and the excited states under the hexagonal CEF. On the other hand, the hardening of C_{66} below T_N is not reproduced, reflecting that the interlevel quadrupole interaction becomes weak in the ordered state due to the splitting of the CEF states by a local internal magnetic field of the AFM ordering. In addition, C_{11} is affected by the elastic behaviors of $(C_{11} - C_{12})/2$ which degenerates with C_{66} in the hexagonal symmetry. The slight softening of C_{11} below 50 K might be due to the quadrupole interaction corresponding to $(C_{11} - C_{12})/2$ [25,34]. The reason why we adopted the singlet ground state will be discussed in Sec. III D.

D. Magnetic field-temperature phase diagram

To investigate the ordered state under magnetic fields in $Tb_3Ru_4Al_{12}$, we carried out ultrasonic measurements under fields. Figures 5(a) and 5(b) show the T and H dependencies of the elastic modulus C_{66}, respectively, along $H||[100]$. An elastic hardening is detected at T_N in the T dependencies of C_{66} up to 6 T. T_N decreases by applying H as is the case with the magnetic susceptibility shown in Fig. 1(a). Above 1 T a broad minimum appears around 30 K. The broad minimum of the transverse modulus was also observed in the isomorphic compound $Dy_3Ru_4Al_{12}$ [20]. The interlevel quadrupole interaction depends on the energy splitting and the magnitude of the matrix elements between the ground and excited states of the CEF and is changed by the Zeeman energy. The broad minimum might appear as the result of a balance between the softening owing to the interlevel quadrupole interaction and the background stiffness. As shown in Fig. 5(b), the H dependence of C_{66} at 2 K exhibits an abrupt hardening at approximately 6.2 T. The magnetic field of the hardening decreases with increasing T. There is no clear anomaly above T_N.

The H dependencies of C_{11} are shown in Fig. 5(c). The modulus C_{11} displays a sharp downward peak at the phase boundary of T_N. The peak becomes broad at 15 K and disappears at 25 K. From the T and H dependencies of the elastic moduli and the magnetic susceptibility, we plotted the H-T phase diagram of $Tb_3Ru_4Al_{12}$ for [100], as shown in Fig. 5(d). T_N decreases monotonically with increasing H and the phase boundary closes around 6.2 T, consisting with the AFM ordered state.

Figures 6(a) and 6(b) show the T and H dependencies of the elastic modulus C_{33}, respectively, along $H||[001]$. The T dependence of C_{33} at 0 T exhibits an elastic hardening at T_N.

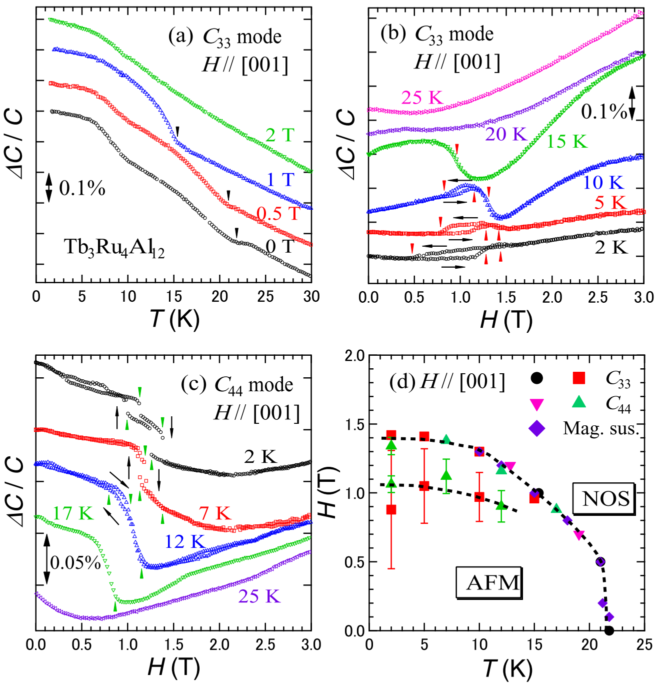

FIG. 6. T and H dependencies of the elastic moduli (a) and (b) C_{33} and (c) C_{44} along $H||[001]$ at various conditions in $Tb_3Ru_4Al_{12}$. We plotted $\Delta C/C$ by adding a constant value to easily see each data curve. The arrows indicate the phase transitions. (d) The H-T phase diagram along $H||[001]$. The broken curves are guides for the eyes. The middle point of hysteresis is defined as the phase transition, and hysteresis is depicted by an error bar. Black circles and magenta down triangles (red squares and green up triangles) represent the phase boundary determined by the T (H) dependencies of the elastic moduli.

The temperature of the hardening decreases with increasing H up to 1 T, and there is no anomaly in the data at 2 T down to 2 K. Two clear elastic anomalies are detected in the H dependencies of C_{33} below 10 K, as shown in Fig. 6(b). The anomaly around 1 T is accompanied by visible hysteresis. These behaviors are consistent with the experimental data of M curves [12,14]. Above 20 K no clear hysteresis is observed.

As shown in Fig. 6(c), the H dependencies of C_{44} display an elastic softening accompanied by visible hysteresis around 1 T. There are two anomalies in C_{44} below 12 K as well as in C_{33}. The magnetic fields of the anomalies decrease with increasing T, and no anomaly is seen at 25 K. From these results including the magnetic susceptibility, we obtained the H-T phase diagram of $Tb_3Ru_4Al_{12}$ for [001], as shown in Fig. 6(d). The AFM phase boundary closes around 1.4 T. In the AFM ordered state, another phase boundary of first order exists around 1 T, and it becomes unclear above 12 K. There is a possibility that this phase transition arises from modulation of the magnetic structure, because M curve shows a step anomaly around this field [12,14].

Hereafter, we focus on the influence of electric quadrupoles in $Tb_3Ru_4Al_{12}$. The elastic softening of C_{66} at zero field indicates that the quadrupole interaction of O_{xy} or O_2^2 is stronger than that of other quadrupoles in $Tb_3Ru_4Al_{12}$ in contrast to $Dy_3Ru_4Al_{12}$ and $Ho_3Ru_4Al_{12}$, which show a large

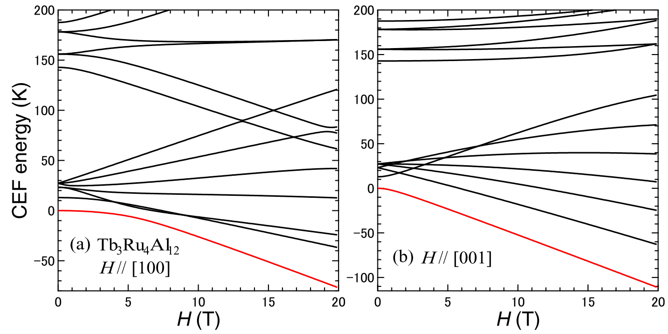

FIG. 7. The H dependencies of the calculated CEF energies along (a) $H||[100]$ and (b) $H||[001]$. The ground singlet is depicted by the red solid curve.

elastic softening of C_{44} with an antiferroquadrupolar-type interaction [19,20,22]. This means that a coupling constant of the quadrupole interaction of O_{yz} or O_{zx} corresponding to C_{44} is relatively small in $Tb_3Ru_4Al_{12}$. The sign of g' in $Tb_3Ru_4Al_{12}$ (C_{66}, positive) is also different from that in $Dy_3Ru_4Al_{12}$ and $Ho_3Ru_4Al_{12}$ (C_{44}, negative), however, the origin of these differences is unclear at present.

On the other hand, under magnetic fields, the energy splitting between the ground and excited CEF states by the Zeeman energy should be considered for understanding the magnitude of magnetic and quadrupole interactions in $Tb_3Ru_4Al_{12}$. We calculated the H dependencies of the CEF energies, which were calculated using $H_{\mathrm{CEF}} + H_{\mathrm{Zeeman}}$, as shown in Figs. 7(a) and 7(b). Along $H||[100]$, the ground state and the excited states possessing the interlevel magnetic and quadrupole interactions separate gradually by applying H, suggesting that the interactions become weak by H. Then T_N decreases monotonically with increasing $H||[100]$, as shown in Fig. 5(d). By contrast, the excited states do not approach the ground state, and the first excited singlet parts from the ground state rapidly by applying $H||[001]$, as shown in Fig. 7(b). Therefore, the AFM phase boundary shown in Fig. 6(d) closes at low field along $H||[001]$.

In the isomorphic compound $Dy_3Ru_4Al_{12}$, the field-induced quadrupolar ordering emerges along both $H||[100]$ and $H||[001]$ [20]. This is because the excited state approaches the ground state and the quadrupole interaction is enhanced with increasing H. In $Tb_3Ru_4Al_{12}$, the excited states part from the ground state by applying H, then no field-induced phase transition appears.

Last, we discuss about the singlet ground state in $Tb_3Ru_4Al_{12}$. In our CEF analyses, the CEF level scheme shown in Fig. 4(c) is the best in order to reproduce a characteristic upturn of M below 6–7 T in the (001) plane [12], because the interlevel spin interactions of J_x and J_y exist between the singlets (Γ_1 and Γ_2) and the second excited doublet Γ_6. In case of the doublet ground state, we have not found CEF parameters to reproduce the characteristic upturn of M in the (001) plane. In addition, the H dependencies of the CEF energies shown in Figs. 7(a) and 7(b) can also explain the anisotropic field dependencies of T_N in the H-T phase diagrams of $Tb_3Ru_4Al_{12}$, as mentioned above. For these reasons, we adopted this CEF level scheme. This makes $Tb_3Ru_4Al_{12}$ a unique compound forming the ground singlet and first excited singlet states, despite that the magnetic transition occurs and the quadrupole interaction exists obviously.

IV. CONCLUSION

We performed ultrasonic measurements on a $Tb_3Ru_4Al_{12}$ single crystal down to 2 K and up to 10 T. The transverse modulus C_{66} shows an obvious elastic softening at zero field. By theoretical analyses of C_{66}, magnetic susceptibilities, and magnetization curves using the hexagonal CEF model, we clarified that the softening is caused by the interlevel quadrupole interaction. We proposed the CEF level scheme: the ground singlet and the first excited singlet separated by 13 K, hence, the AFM ordering originates from the interlevel spin interaction. The anisotropic H-T phase diagrams for [100] and [001] were also clarified, and those can be qualitatively understood by the CEF model.

ACKNOWLEDGMENTS

This work was supported by JSPS KAKENHI Grants No. 17H06136, No. 18KK0078, and No. 19K03719. This work was also supported by CResCent (Chirality Research Center) in Hiroshima University (the MEXT program for promoting the enhancement of research universities, Japan) and by JSPS Core-to-Core Program, A. Advanced Research Networks. The work was supported by Projects No. 19-00925S and No. 19-07931Y of the Czech Science Foundation and by MGML within the Program of Czech Research Infrastructures (Project No. LM2018096). We acknowledge the support of High Magnetic Field Laboratory (HLD) at Helmholtz-Zentrum Dresden-Rossendorf (HZDR), a member of the European Magnetic Field Laboratory (EMFL). A part of this work was also funded by the National Sustainability Programme I of Czech Republic (Project No. LO1603) under the Ministry of Education, Youth, and Sports.

[1] H. Sato, H. Sugawara, Y. Aoki, and H. Harima, in *Handbook of Magnetic Materials*, Vol. 18, edited by K. H. J. Buschow (North Holland, Amsterdam, 2009), Chap. 1.

[2] T. Onimaru and H. Kusunose, J. Phys. Soc. Jpn. **85**, 082002 (2016).

[3] A. P. Ramirez, Annu. Rev. Mater. Sci. **24**, 453 (1994).

[4] R. Moessner and A. P. Ramirez, Phys. Today **59**(2), 24 (2006).

[5] J. Niermann and W. Jeitschko, Z. Anorg. Allg. Chem. **628**, 2549 (2002).

[6] W. Ge, H. Ohta, C. Michioka, and K. Yoshimura, J. Phys.: Conf. Ser. **344**, 012023 (2012).

[7] D. I. Gorbunov, M. S. Henriques, A. V. Andreev, V. Eigner, A. Gukasov, X. Fabrèges, Y. Skourski, V. Petříček, and J. Wosnitza, Phys. Rev. B **93**, 024407 (2016).

[8] T. Suzuki, T. Mizuno, K. Takezawa, S. Kamikawa, A. V. Andreev, D. I. Gorbunov, M. S. Henriques, and I. Ishii, Physica B **536**, 18 (2018).

[9] M. S. Henriques, D. I. Gorbunov, A. V. Andreev, X. Fabrèges, A. Gukasov, M. Uhlarz, V. Petříček, B. Ouladdiaf, and J. Wosnitza, Phys. Rev. B **97**, 014431 (2018).

[10] S. Nakamura, N. Kabeya, M. Kobayashi, K. Araki, K. Katoh, and A. Ochiai, Phys. Rev. B **98**, 054410 (2018).

[11] T. Matsumura, Y. Ozono, S. Nakamura, N. Kabeya, and A. Ochiai, J. Phys. Soc. Jpn. **88**, 023704 (2019).

[12] D. I. Gorbunov, M. S. Henriques, A. V. Andreev, Y. Skourski, and M. Dušek, J. Alloys Compd. **634**, 115 (2015).

[13] S. K. Upadhyay, K. K. Iyer, and E. V. Sampathkumaran, J. Phys.: Condens. Matter **29**, 325601 (2017).

[14] E. V. Sampathkumaran, K. K. Iyer, S. K. Upadhyay, and A. V. Andreev, Solid State Commun. **288**, 64 (2019).

[15] S. Rayaprol, A. Hoser, K. K. Iyer, S. K. Upadhyay, and E. V. Sampathkumaran, J. Magn. Magn. Mater. **477**, 83 (2019).

[16] D. I. Gorbunov, M. S. Henriques, A. V. Andreev, A. Gukasov, V. Petříček, N. V. Baranov, Y. Skourski, V. Eigner, M. Paukov, J. Prokleška, and A. P. Gonçalves, Phys. Rev. B **90**, 094405 (2014).

[17] M. S. Henriques, D. I. Gorbunov, D. Kriegner, M. Vališka, A. V. Andreev, and Z. Matěj, J. Magn. Magn. Mater. **400**, 125 (2016).

[18] V. Chandragiri, K. K. Iyer, and E. V. Sampathkumaran, Intermetallics **76**, 26 (2016).

[19] I. Ishii, K. Takezawa, H. Goto, S. Kamikawa, A. V. Andreev, D. I. Gorbunov, M. S. Henriques, and T. Suzuki, J. Phys.: Conf. Ser. **807**, 012002 (2017).

[20] I. Ishii, T. Mizuno, K. Takezawa, S. Kumano, Y. Kawamoto, T. Suzuki, D. I. Gorbunov, M. S. Henriques, and A. V. Andreev, Phys. Rev. B **97**, 235130 (2018).

[21] S. Gao, M. Hirschberger, O. Zaharko, T. Nakajima, T. Kurumaji, A. Kikkawa, J. Shiogai, A. Tsukazaki, S. Kimura, S. Awaji, Y. Taguchi, T. H. Arima, and Y. Tokura, Phys. Rev. B **100**, 241115(R) (2019).

[22] D. I. Gorbunov, T. Nomura, I. Ishii, M. S. Henriques, A. V. Andreev, M. Doerr, T. Stöter, T. Suzuki, S. Zherlitsyn, and J. Wosnitza, Phys. Rev. B **97**, 184412 (2018).

[23] S. Nakamura, S. Toyoshima, N. Kabeya, K. Katoh, T. Nojima, and A. Ochiai, Phys. Rev. B **91**, 214426 (2015).

[24] D. I. Gorbunov, I. Ishii, T. Nomura, M. S. Henriques, A. V. Andreev, M. Uhlarz, T. Suzuki, S. Zherlitsyn, and J. Wosnitza, Phys. Rev. B **99**, 054413 (2019).

[25] T. Suzuki, I. Ishii, N. Okuda, K. Katoh, T. Takabatake, T. Fujita, and A. Tamaki, Phys. Rev. B **62**, 49 (2000).

[26] Y. Nemoto, T. Yamaguchi, T. Horino, M. Akatsu, T. Yanagisawa, T. Goto, O. Suzuki, A. Dönni, and T. Komatsubara, Phys. Rev. B **68**, 184109 (2003).

[27] Y. Nakanishi, T. Sakon, M. Motokawa, M. Ozawa, T. Suzuki, and M. Yoshizawa, Phys. Rev. B **68**, 144427 (2003).

[28] T. Yanagisawa, T. Goto, Y. Nemoto, S. Miyata, R. Watanuki, and K. Suzuki, Phys. Rev. B **67**, 115129 (2003).

[29] T. Goto, Y. Nemoto, K. Sakai, T. Yamaguchi, M. Akatsu, T. Yanagisawa, H. Hazama, K. Onuki, H. Sugawara, and H. Sato, Phys. Rev. B **69**, 180511(R) (2004).

[30] M. Akatsu, T. Goto, O. Suzuki, Y. Nemoto, S. Nakamura, S. Kunii, and G. Kido, Phys. Rev. Lett. **93**, 156409 (2004).

[31] I. Ishii, H. Muneshige, Y. Suetomi, T. K. Fujita, T. Onimaru, K. T. Matsumoto, T. Takabatake, K. Araki, M. Akatsu, Y. Nemoto, T. Goto, and T. Suzuki, J. Phys. Soc. Jpn. **80**, 093601 (2011).

[32] I. Ishii, H. Muneshige, S. Kamikawa, T. K. Fujita, T. Onimaru, N. Nagasawa, T. Takabatake, T. Suzuki, G. Ano,

M. Akatsu, Y. Nemoto, and T. Goto, Phys. Rev. B **87**, 205106 (2013).
[33] S. Kamikawa, I. Ishii, K. Takezawa, T. Mizuno, T. Sakami, F. Nakagawa, H. Tanida, M. Sera, T. Suzuki, K. Mitsumoto, and X. Xi, Phys. Rev. B **96**, 155131 (2017).
[34] I. Ishii, K. Takezawa, T. Mizuno, S. Kamikawa, H. Ninomiya, Y. Matsumoto, S. Ohara, K. Mitsumoto, and T. Suzuki, J. Phys. Soc. Jpn. **87**, 013602 (2018).
[35] I. Ishii, K. Takezawa, T. Mizuno, S. Kumano, T. Suzuki, H. Ninomiya, K. Mitsumoto, K. Umeo, S. Nakamura, and S. Ohara, Phys. Rev. B **99**, 075156 (2019).
[36] D. I. Gorbunov, A. V. Andreev, I. Ishii, K. Prokeš, T. Suzuki, S. Zherlitsyn, and J. Wosnitza, Phys. Rev. B **101**, 014408 (2020); Editors' Suggestion.
[37] T. J. Moran and B. Lüthi, Phys. Rev. **187**, 710 (1969).
[38] B. Lüthi, in *Dynamical Properties of Solids*, edited by G. K. Horton and A. A. Maradudin (North-Holland, Amsterdam, 1980), Chap. 4.
[39] Y. P. Varshni, Phys. Rev. B **2**, 3952 (1970).
[40] Z. Zhang, V. Keppens, and T. Egami, J. Appl. Phys. **102**, 123508 (2007).
[41] M. Sera, H. Nohara, M. Nakamura, H. Tanida, T. Nishioka, and M. Matsumura, Phys. Rev. B **88**, 100404(R) (2013).
[42] N. V. Hieu, T. Takeuchi, H. Shishido, C. Tonohiro, T. Yamada, H. Nakashima, K. Sugiyama, R. Settai, T. D. Matsuda, Y. Haga, M. Hagiwara, K. Kindo, S. Araki, Y. Nozue, and Y. Ōnuki, J. Phys. Soc. Jpn. **76**, 064702 (2007).
[43] S. Kamikawa, I. Ishii, Y. Noguchi, H. Goto, T. K. Fujita, F. Nakagawa, H. Tanida, M. Sera, and T. Suzuki, J. Phys. Soc. Jpn. **85**, 074604 (2016).